Review

Dexrazoxane: Exposing the Vulnerability of SARS-CoV-2

Keith McCormack

McCormack Pharma, a division of McCormack Ltd, Stirling House, 9 Burroughs Gardens, London NW4 4AU, UK; keithmccormack@mccormack-group.com

Abstract: In 2018, the author identified a previously unknown/unreported association between dexrazoxane and poly(ADP-ribose) (PAR). Interestingly, PAR is a close structural analogue of the polyadenine nucleotide polymer, polyadenosine monophosphate (poly(A)). In this report, subsequent *in silico* modelling of the interaction between dexrazoxane and poly(A) reveals some notable differences from the previously reported interaction between dexrazoxane and PAR. Significantly, the supramolecular self-assembly of dexrazoxane and poly(A) is distinguished by vertically-orientated nonelectrostatic forces comparable to the stabilizing interactions between stacked bases within DNA. Notably, the vertical separation of 3.4 Å between each stack is consistent with solvent entropy as a dominant driving force in stabilising the interaction. Additionally, concomitant conformational analysis by the author reveals the existence of low energy planar conformers of dexrazoxane. This analysis enables an explanation for the considerable discrepancies and conflicts that exist within the reported pharmacokinetic data for dexrazoxane. Exploring the significance of the interaction between dexrazoxane and poly(A), the author illustrates that survival, translation and replication of the severe acute respiratory syndrome virus 2 (SARS-CoV-2) is absolutely dependent upon the mature and unhindered poly(A) tail of the SARS-CoV-2 genome. The proposition herein, that dexrazoxane, as a chameleonic agent sequesters the poly(A) tail of the SARS-CoV-2 genome by the catalysis of a supramolecular hybrid assembly establishes SARS-CoV-2 infected cells as deep compartments for the accumulation of dexrazoxane. Taken together, dexrazoxane or its demethylated analogue, represent a novel treatment to kill the SARS-CoV-2 virus by irreversible destabilization of the SARS-CoV-2 poly(A) tail.

Key Points:

- Survival and replication of the SARS-CoV-2 virus are critically dependent upon an intact repetitive sequence of adenine nucleotides at the 3′ terminus, known as the poly(A) tail.
- *In silico* modelling by the author of stacking of planar conformational isomers of dexrazoxane, and non-covalent interactions between dexrazoxane and the poly(A) tail suggests that SARS-CoV-2 infected cells represent a deep compartment for the accumulation of dexrazoxane molecules.
- The author shows that non-covalent forces that include canonical and non-canonical base pairing, and base stacking between dexrazoxane molecules and adjacent poly(A) tails of individual SARS-CoV-2 viruses result in the self-assembly of a thermodynamically favoured supramolecular construct which, the author proposes destabilizes the poly(A) tail rendering the SARS-CoV-2 virus incapable of normal function and replication.

Keywords: SARS-CoV-2; Poly(A); dexrazoxane; supramolecular self-assembly; base stacking

1. Introduction to dexrazoxane

Historical aspects

Readers interested in the clinical development of dexraxoxane are referred to publications by Hasinoff [1] and Herman [3-7].

Preprints (www.preprints.org) | NOT PEER-REVIEWED | Posted: 9 December 2022 doi:10.20944/preprints202212.0175.v1

Physical properties and clinical application

Under the rules of IUPAC nomenclature, dexrazoxane (ICRF-187) is described as 4-[(2*S*)-2-(3,5-dioxopiperazin-1-yl)propyl]piperazine-2,6-dione (Figure 1). Using non-systematic nomenclature dexrazoxane is also classified as a bis(2,6-diketopiperazine) or a bisdioxopiperazine. Each of these classifications is subsumed more generally within the category of cyclic dipeptides. Dexrazoxane is < 2% bound to plasma proteins, and at physiological pH levels in the region of pH 7 or thereabouts, the pKa values shown in figure 1 for each ionizable/protonatable group are consistent with the description of dexrazoxane as a lipophilic drug [2].

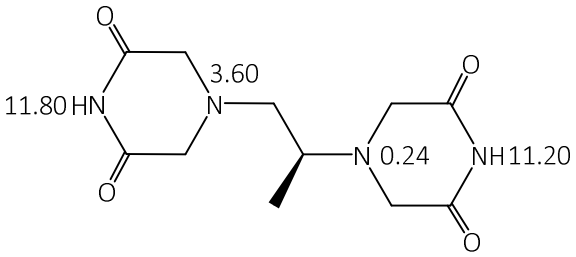

Figure 1. Dexrazoxane (ICRF-187) 4-[(2S)-2-(3,5-dioxopiperazin-1-yl)propyl]piperazine-2,6-dione. pKa values are shown adjacent to each ionizable/protonable group.

In the UK, dexrazoxane (Cardioxane) is indicated for use…. "in adults for the prevention of chronic cumulative cardiotoxicity caused by anthracycline use"… "in advanced and/or metastatic breast cancer patients" (emc Section 4.1) [8].

2. About dexrazoxane

Part I of IV

How does dexrazoxane transfer acoss cell membranes?

Contradictions and conflicts in the pharmacokinetic characterization of dexrazoxane

Following intravenous administration of 500 mg m^{-2}, dexrazoxane distributes rapidly into tissue fluids with an estimated mean steady-state volume of distribution of 25 L m^{-2} which, it is claimed, is consistent with distribution primarily within the total body water [8-11]. But is this a reasonable claim?

The mean peak plasma concentration of dexrazoxane is reported as 36.5 μg ml^{-1} at fifteen minutes following intravenous administration of a 500 mg m^{-2} dose [9-12]. The total body water of a 70 kg middle-aged man is approximately 42 L. Accordingly, with a plasma concentration of dexrazoxane of 36.5 μg ml^{-1}, and assuming rapid distribution within the total body water compartment, the absolute number of dexrazoxane molecules within a total body water volume of 42 L is approximately 10^{20}. Administration of a dose of dexrazoxane of 500mg m^{-2} in a man with a body surface area of 1.8 m^2 is equal to 10^{21} molecules. Taken together, these calculations show close approximation between the number of molecules of dexrazoxane administered and the number that is presumed to distribute within the total body water of 42 L.

Thus, given that the apparent volume of distribution of dexrazoxane is reported as 25 L m^{-2} then the above calculations support the consensus that the distribution of dexrazoxane is primarily within the total body water [8-11].

Physically, pure dexrazoxane is sparingly/poorly soluble in water [9,13]. Paradoxically, reports of macroscopic log P values calculated using various atom-additive algorithms, yield values of -1.0, -1.4, -2.14, -2.6 and -2.7 [9, 14-17]. Accordingly, rapid distribution of dexrazoxane within the total body water, of which 23 L is intracellular water, appears to be incompatible with negative values of log P of this magnitude that typically characterize membrane impermeable molecules [18]. In isolation, these results suggest

 doi:10.20944/preprints202212.0175.v1

that dexrazoxane is very hydrophilic, which is difficult to reconcile with the empirical observation of dexrazoxane as a sparingly/poorly soluble drug in water.

However, substantial hydrophilic character as suggested by the above log P values does accord with the empirical observation that dexrazoxane is insoluble in non-polar solvents [9-11]. Lack of solubility in non-polar solvents makes it is difficult to understand how dexrazoxane can rapidly distribute across cell membrane lipids and gain access to the intracellular water compartment.

For most small molecules, size and polarity determine the rate of transmembrane diffusion, whereby membrane permeability is inversely related to topological polar surface area (TPSA). For example, the TPSA value of 20.2 Å² for ethanol is entirely consistent with this molecule's high permeability [19-22]. However, with a small increase in size, polar molecules such as urea and glycerol with TPSA values of 69.1 Å² [27] and 60.7 Å² [24] respectively, both demonstrate reduced permeability [25,26] (Yang and Hinner, 2015) [71].

Consequently, the TPSA value for dexrazoxane of 98.8 Å² [9] appears inconsistent with rapid uptake and distribution in tissues given that, as discussed above, the volume of distribution for dexrazoxane is consonant with distribution within the total body water of 40 to 42 L of which approximately 23 L is intracellular water.

Collectively, the most parsimonious explanation, as argued below, is that in a context-dependent manner dexrazoxane can assume conformations with varying degrees of lipid solubility. As elegantly overviewed by Batista and coworkers [28] and Matsson and Kihlberg [72] the concept of environment-dependent conformations, also known as chameleonic behaviour [73] is characterised by molecules with the capacity to assume conformations with differing degrees of lipid-permeability and aqueous-solubility. Lipid-permeable conformations display lower TPSA values and aqueous-soluble conformation display higher TPSA values (Matsson and Kihlberg, 2015) [72].

3. About dexrazoxane

Part II of IV

Conformational analysis of dexrazoxane

What are conformational isomers?

Conformational isomers exist when atoms rotate about single bonds. Interconversion from one conformer to another requires that rotations need to overcome an energy barrier. Importantly, molecules with rotatable bonds must not be considered as a static entity, but rather it is necessary to embrace the burgeoning concept that these so-called "flexible" molecules occupy a space within which there exists wide-ranging and dynamic conformational freedom

Quantifying conformational isomers

In the presence of conformers, a single log P value represents macroscopic or apparent lipophilicity [29]. In a 1979 publication, Davies and coworkers at the Pharmaceutical Division of ICI in Alderly Park, United Kingdom recognised that in the presence of multiple conformers, the dominant conformer is not necessarily the active agent. Accordingly, the contribution of minor conformers in determining pharmacological activity must be incorporated into a unifying model of "micropartition coefficients" (Davies et al, 1979 p. 397)[30]. Notably, that such micropartition coefficients underscore chameleonic behaviour was eruditely illustrated by the labours of Testa and co-workers in the Institut de Chimie Therapeutic at the Universite de Lausanne in Switzerland [31,32], who examined a range of conformers of morphine glucuronides and concluded that the behaviour of morphine glucuronide in different liquid phases could be appropriately defined as "chameleonic" (David et al, 2021) [73]. That is, they propose that their results support the existence of an equilibrium between hydrophilic conformers of morphine glucuronide in water, and more lipophilic conformers within lipid structures such as cell membranes [31,32].

 doi:10.20944/preprints202212.0175.v1

Conformational isomerism translates into pharmacological activity

In the clinic, dexrazoxane is available in powder form as the water-soluble protonated hydrochloride salt for reconstitution prior to intravenous administration. The pH of the reconstituted product is 1.6, which is further diluted before administration [8], yielding infusion solutions with a pH in the range of 3.5 to 5.5 [15]. Within the systemic circulation at the higher pH 7.4, dexrazoxane rapidly becomes deprotonated and circulates as a wholly unionized species. However, given the considerable dilution factor within a plasma volume of several litres, then dexrazoxane remains in solution despite the limited aqueous solubilty demonstrated in a laboratory setting. But as the author now illustrates, it is the equilibrium between circulating free (< 2% bound to plasma proteins) monomeric unionized dexrazoxane, and stacked conformers of dexrazoxane that confer pharmacological activity given the enhanced lipid solubility of stacked dexrazoxane (discussed below). It is the existence of stacked conformers that provides considerable insight in reconciling the discrepancies and conflicts apparent within the reported pharmacokinetic data for dexrazoxane.

Dexrazoxane has three rotatable bonds

Dexrazoxane is a flexible molecule that possesses three rotatable bonds [9].

Conformational analysis of dexrazoxane by the author demonstrates energy barriers to free rotation that are low resulting in a highly dynamic and rapidly equilibrating mixture of multiple low-energy conformational isomers (Figure 2). Indeed, the conformational free energy landscape of dexrazoxane illustrates the complexity in low molecular weight organic molecules that possess multiple rotatable bonds.

To the author's knowledge there are no reports evident within the available literature of conformational analysis of dexrazoxane other than that performed by the author in 2014 and briefly reported in 2018 [33]. That this feature of dexrazoxane has been overlooked, at least within the published literature, is noteworthy given that the rotatable bond content of dexrazoxane is documented and publicly available within the National Library of Medicine of the National Center for Biotechnology Information [9].

Taken together, this analysis suggests that, as discussed below, it is stacked planar dexrazoxane conformers that is the most membrane permeable form.

Preprints (www.preprints.org) | NOT PEER-REVIEWED | Posted: 9 December 2022 doi:10.20944/preprints202212.0175.v1

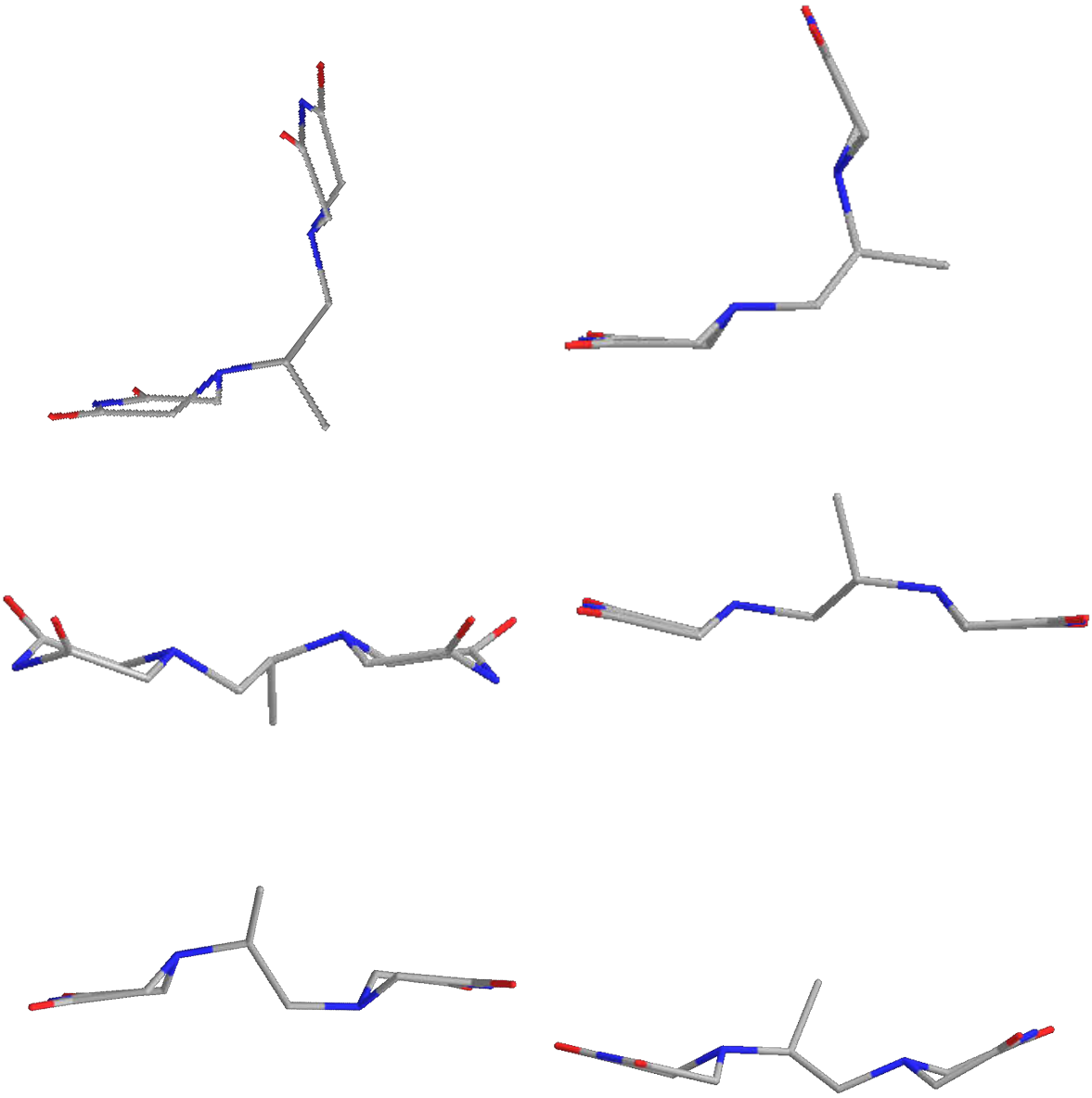

Figure 2. Dexrazoxane is a flexible molecule that possesses three rotatable bonds resulting in numerous conformational isomers (conformers). A few examples of low-energy conformers are illustrated above.

4. About dexrazoxane

Part III of IV

The case for stacked parallel conformers of dexrazoxane as the membrane permeable form

Why is stacking an energetically favoured process?

Generally, the driving force for supramolecular assembly does not result from any favourable interaction between stacked hydrophobic surfaces, as it is commonly argued, but rather from their thermodynamically unfavourable interaction with water [45-49].

Indeed, stability of the DNA double helix is more dependent upon base stacking than base pairing [39]. Free bases (adenine, thymine, cytosine and guanine) in water stack vertically in preference to forming horizontally-orientated hydrogen-bonded pairs [40-43]. Using a Monte Carlo algorithm, the computational simulations of Danilov and co-workers at the Institute of Molecular Biology and Genetics at the National Academy of

 doi:10.20944/preprints202212.0175.v1

Sciences of Ukraine, in Kyiz [40] show that stacked base dimers (adenine-thymine; adenine-uracil; guanine-cytosine) are thermodynamically preferable by comparison with the corresponding Watson-Crick hydrogen-bonded base pairs.

Importantly, solvent molecules (water) and solute molecules cannot occupy the same space and a solute excludes solvent molecules from the volume that it occupies. The elegant simulations of Mak and co-workers [45] in the Department of Chemistry and Center of Applied Mathematical Sciences at the University of Southern California, USA show that as two bases approach each other to form a vertical stack there is a maximum release of energy as described by a minimum value of Gibbs free energy at a distance between the bases of 3.4 Å. This of course is the distance between stacked bases within DNA, and Mak's simulations [45] confirm that base stacking is a spontaneous process with maximum stability between bases at a distance of 3.4 Å. Mak and co-workers also demonstrate that stacked bases can only be separated with an input of energy.

Crucially, the study by Mak and co-workers reveals that the magnitude of the solvent entropy-driven base stacking force is directly related to the size (volume) of a cavity within the solvent, and that the stability of the base stack is proportional to the size of the bases (the relevance of this finding to dexrazoxane is discussed below).

Dexrazoxane is a chameleonic molecule

Although the number of polar groups in a molecule is directly related to aqueous solubility, an inverse relationship exists between the content of polar groups and membrane permeability. Consequently, polarity is an important consideration in traditional assessments of a molecule's candidacy for usefulness as a therapeutic agent [34].

Chameleonic behaviour is eruditely defined by David and workers [73] as "the capacity of a molecule to hide polarity in non-polar environments (such as when traversing lipid membranes) and expose it in water" (David et al 2021,) [73]. That is, surface polarity as measured by TPSA, is environment dependent.

These new teachings provide an opportunity to reconcile conflicts between physical properties and pharmacokinetic parameters for selected molecules.

The author proposes that dexrazoxane is a chameleonic molecule whereby the monomeric structure with hydrogen bond donors fully exposed exhibits extensive solvation in an aqueous environment. This "open" structure is in equilibrium with stacked dexrazoxane (Figure 3) whereby polar groups are buried rendering the stacked assembly lipophilic and more able to diffuse across a plasma membrane. That is, since TPSA is a surface area phenomenon, then a low ratio of TPSA to stack size characterizes an efficient assembly for the consolidated transport of several molecules of dexrazoxane through a lipidic environment.

Dexrazoxane is a structural analogue of bis-thymine

Interestingly, consonant with the observations reported above, Luo and coworkers [41] have demonstrated stacking of adenine bases when joined by a three carbon atom linker (bis-adenyl) (Figure 4). This is noteworthy, given the striking figurative similarity between bis-adenyl, dexrazoxane, and two thymine bases linked symmetrically by a 1-methyl-1,2-ethanediyl linker at carbon atom 6 of each thymine base (bis-thymine) (Figure 4) [44].

Absolute planarity of a nucleobase is not a prerequisite for parallel stacking

Importantly, conformational analysis of dexrazoxane also reveals that at methylene carbon atoms 3 and 5, each piperazine structure occupies a half-chair conformation resulting in an elevated tertiary amine nitrogen atom (previously reported by the author in [33] (Figure 2). This observation raises the important question whether this lack of planarity within each piperazine structure compromises the chameleonic equilibrium for dexrazoxane presented above?

Preprints (www.preprints.org) | NOT PEER-REVIEWED | Posted: 9 December 2022 doi:10.20944/preprints202212.0175.v1

In addressing this issue, it is instructive to review the work by Olexandr Isayev and coworkers at the Computational Center for Molecular Structure and Interactions at Jackson State University in Mississippi, USA [35]. These workers challenged the prevailing view that isolated nucleic acid bases exist as planar conformations. Using *ab-initio* Car-Parrinello molecular dynamics simulations of the flexibility of isolated DNA bases they demonstrated that all nucleic acid bases are highly flexible molecules and that cytosine, thymine and uracil possess a non-planar conformation of the pyrimidine ring with the boat-like and half-chair conformations representing the most populated conformations. This is an illuminating observation by Isayez and coworkers, given that paradoxically, it is the planar geometry that occupies a minimum value on the potential energy surface. The assumption that nucleic acid bases are absolutely planar and conformationally rigid structures has been challenged by other groups [36-38]. Indeed, the historical concept of base planarity is not consistent with recent experimental observations [38], and moreover, the consensus today is that base stacking within nucleotide polymers is contingent upon flexibility of nucleic acid bases. Accordingly, it is not unreasonable to accept that the half-chair conformation of each of the piperazine structures of dexrazoxane does not conflict with the concept expressed herein of chameleonic behaviour of dexrazoxane, that includes stacking of parallel conformers of dexrazoxane. Consequently, the definition of "planar" dexrazoxane used by the author incorporates the caveat that each piperazine structure occupies a half-boat conformation.

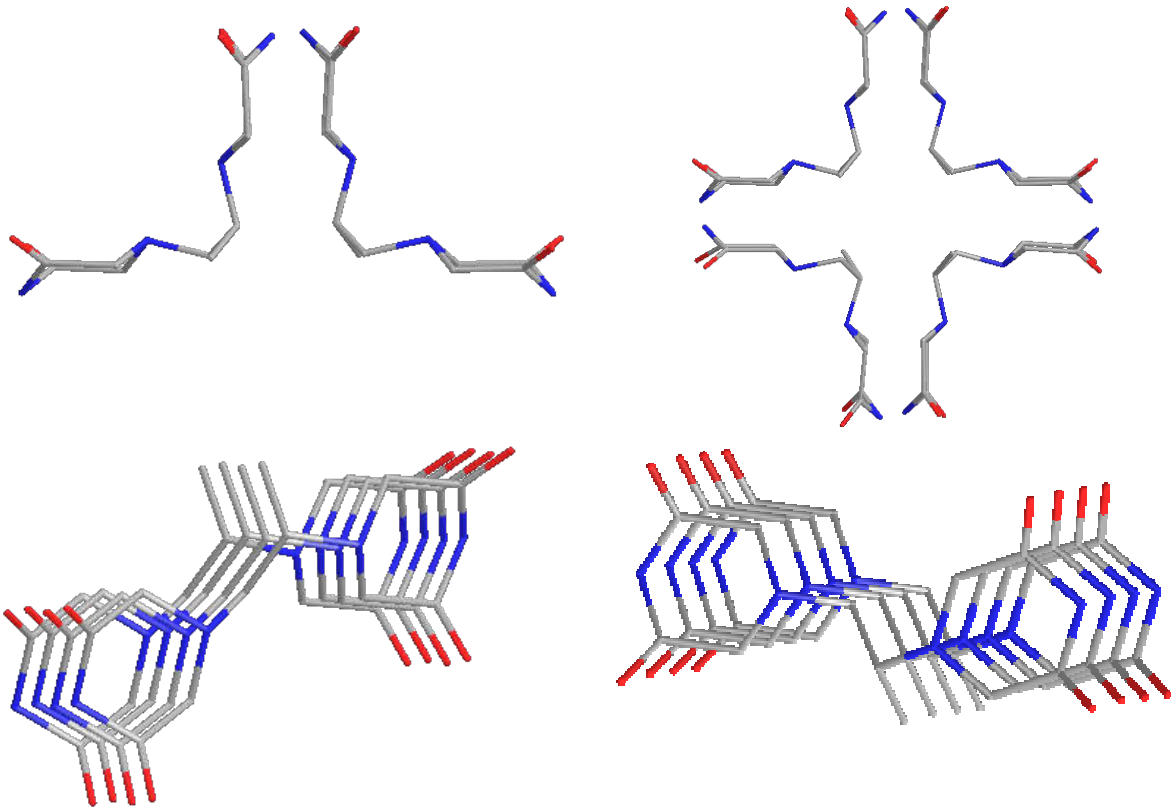

Figure 3. Dexrazoxane is a chameleonic molecule. Polar groups (oxygen in red and nitrogen in blue) are buried within planar stacks resulting in an increase in lipophilicity.

Preprints (www.preprints.org) | NOT PEER-REVIEWED | Posted: 9 December 2022 doi:10.20944/preprints202212.0175.v1

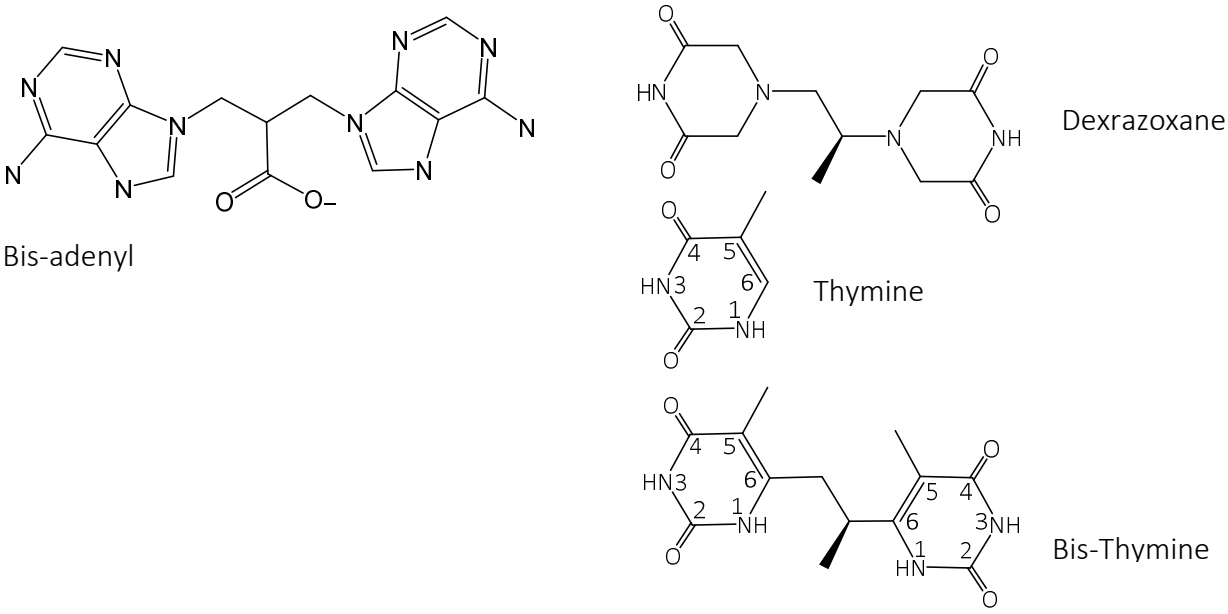

Figure 4. Bis-adenyl consists of two adenine bases separated by a flexible aliphatic linker. Dexrazoxane is analogous to a bis-thymine construct whereby two thymine bases are separated by a 1-methyl-1,2-ethanediyl aliphatic linker, similar to that in dexrazoxane.

Summary

Taken together, it is the author's view that stacking of planar dexrazoxane results in an energetically favourable process that accords with current teachings, especially those that describe the behaviour of nucleic acid bases in water, whether as free structures or dimers.

5. About dexrazoxane

Part IV of IV

Mechanism of action of dexrazoxane

Historically, the mechanism(s) of action of dexrazoxane have been the subject of considerable debate, that notably have focussed upon the ethylenediaminetetraacetic acid (EDTA)-like metabolite of dexrazoxane, ADR-925 with the proposal that as a strong iron chelator, ADR-925 exerts a cardioprotective effect through displacing iron bound to cardiotoxic anthracyclines. However, this theory has not been supported by rigorous scientific scrutiny (For review see [33]).

In recent times, the outcomes of *in vitro* and *in vivo* studies have given rise to the claim, that dexrazoxane protects the heart from the effects of anthracyclines by depleting levels of topoisomerase 2β (Top2β) within cardiomyocytes (For review see [33]).

However, an exhaustive review and analysis by the author reported in 2018 resulted in the conclusion that the evidence does not support this claim [33]. As the author reported in that earlier publication [33]……."At best, the *in vivo* results show that the lowering of Top2β protein level by dexrazoxane is transient and short-lived (hours) with a rapid recovery by newly synthesised Top2β protein" (McCormack, 2018) [33].

The author concludes [33]:

"Within the context of persistently elevated levels of doxorubicin over a period of days and weeks, it is difficult to understand how in a clinical setting lowering of Top2β protein levels following a single 15-minute infusion of dexrazoxane, with a mean half-life of 2.2 hours, can translate into a cardioprotective effect.

Preprints (www.preprints.org) | NOT PEER-REVIEWED | Posted: 9 December 2022 doi:10.20944/preprints202212.0175.v1

Moreover, such a reductionist notion of Top2β protein lowering also fails to explain the long-term (years) cardioprotective effects of dexrazoxane [50] or the quantifiable differences in cell biology between long-term survivors who received doxorubicin by comparison with those who received doxorubicin plus dexrazoxane [51]" [McCormack, 2018) [33].

Dexrazoxane sequesters poly(ADP-ribose) polymer

In 2018, using a customised association rule learning algorithm the author reports a previously-unknown association between dexrazoxane and poly(ADP-ribose) polymer [33]. From that analysis the author concluded that the mechanism of action of dexrazoxane involves an interaction with poly(ADP-ribose) polymer (McCormack, 2018) [33]. Subsequently, *in silico* modelling together with *in vitro* investigations allowed the conclusion by the author that dexrazoxane catalyses the "hybrid self-assembly" (McCormack, 2018) of the nucleic acid biopolymer, poly(ADP-ribose) [33], whereby……"this assembly depicts an antiparallel orientation of canonical Watson-Crick base pairing of dexrazoxane with adenine bases" (McCormack, 2018) [33]; additional stabilising forces were also proposed [33].

Poly(A) is closely related to poly(ADP-ribose)

Given the structural similarity between poly(ADP-ribose) and the polyadenine nucleotide structure of the SARS-CoV-2 genome, known as the poly(A) tail (Figure 5), then dexrazoxane has the capacity to functionally dismantle the virus. This is discussed next.

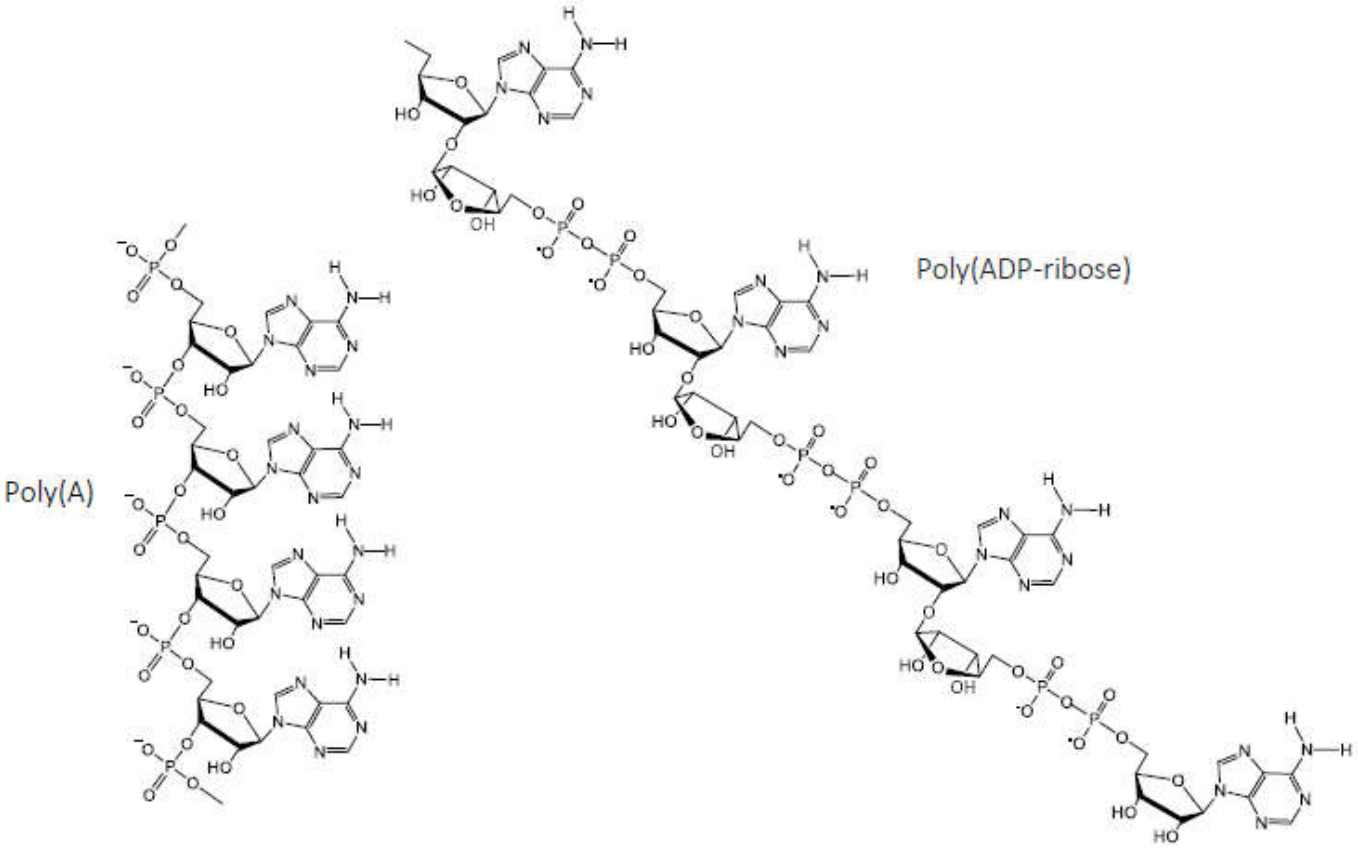

Figure 5. Poly(A) is closely related to poly(ADP-ribose).

Preprints (www.preprints.org) | NOT PEER-REVIEWED | Posted: 9 December 2022 doi:10.20944/preprints202212.0175.v1

6. Dexrazoxane targets the Achille's heel of SARS-CoV-2

SARS-CoV-2

Coronavirus disease 19 (COVID-19) is elicited by severe acute respiratory syndrome coronavirus 2 (SARS-CoV-2). In common with other coronaviruses, SARS-CoV-2 is an enveloped virus with a positive-sense, single-stranded polyadenylated RNA genome of approximately thirty kilobytes that encodes multiple viral proteins.

Introducing polyadenylation and the poly (A) tail

Within the nucleus of eukaryotic cells, the process of transcription results in the novel synthesis of a mRNA copy of a gene sequence from a strand of DNA. Following this, modifications to this nascent mRNA structure are required before the mRNA can be exported to the cytoplasm where ribosomes read the genetic information. A critical modification in the maturation process involves cleavage of the 3′ terminus of the mRNA followed by the addition of a series of adenosine monophosphate units to form a polyadenine nucleotide polymeric (poly(A)) tail (Figure 6) by a process known as polyadenylation. The resulting poly(A) tail enhances stability of the mRNA, protects it from degradation and facilitates transcript stability, nuclear export, and translation.

The mechanism of polyadenylation and the length of the resultant poly(A) tail is a complex process that is modulated by interactions between polyadenylation polymerase, cleavage and polyadenylation specificity factor, and nuclear poly(A)-binding protein (further discussion below).

Most eukaryotic genes contain multiple polyadenylation sites, and a conserved hexameric sequence AAUAAA (A=adenosine, U=uridine) within the 3′-untranslated region that typically directs the addition of adenosine residues that become the poly(A) tail at the 3′ terminus of the mRNA transcript.

In summary, for eukaryotic mRNAs, polyadenylation occurs in the cell nucleus, which is where the mRNA is formed. In addition to its essential function in protecting mRNA from degradation and ensuring its stability, the poly(A) tail is essential for efficient protein production following export from the cellular nucleus to the ribosomal translational and protein synthesis machinery, located within the cytoplasm.

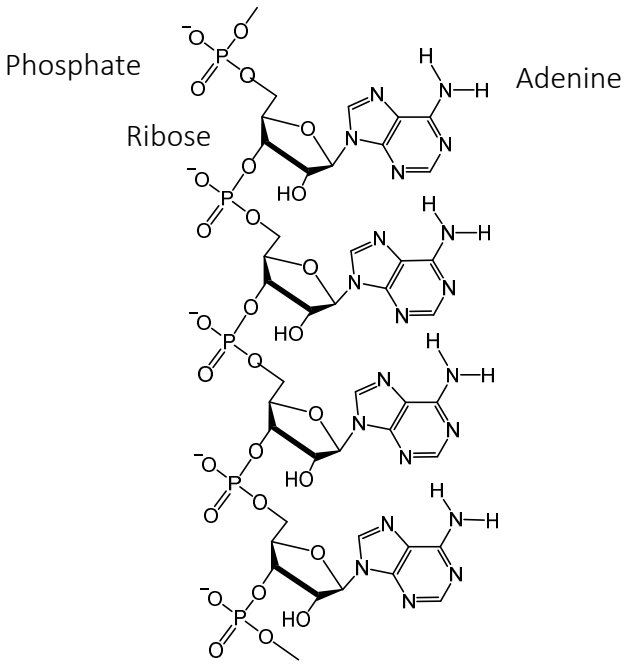

Figure 6. The polyadenine nucleotide structure. Poly(A) is a polymer of adenosine monophosphate (AMP). AMP consists of a phosphate group, ribose, and the nucleobase adenine.

Preprints (www.preprints.org) | NOT PEER-REVIEWED | Posted: 9 December 2022 doi:10.20944/preprints202212.0175.v1

Polyadenylation of coronavirus RNA

In common with eukaryotic mRNA, coronavirus RNA has a poly(A) tail. However, because the life cycle of a coronavirus takes place in the host cytoplasm, and it does not enter the cell nucleus, the temporal and spatial origins of the coronavirus poly(A) tail remain uncertain.

There are few reports that describe SARS-CoV-2 RNA polyadenylation. By combining nanopore-based direct RNA sequencing, and DNA nanoball sequencing, researchers led by Narry Kim and Hyeshik Chang at the Center for RNA Research within the Institute for Basic Science (IBS) in Seoul, present a high-resolution map of the SARS-CoV-2 transcriptome [57]. Using this methodology, they confirm that like other coronaviruses, SARS-CoV-2 RNA carries a poly(A) tail and that the full-length genomic RNA has a relatively longer tail than the shorter subgenomic RNAs.

In common with other coronaviruses, the 3′ untranslated region of SARS-CoV-2 has no canonical polyadenylation signal sequence AAUAAA. However, it has been proposed by Yu-Hui Peng and co-workers at the Graduate Institute of Veterinary Pathobiology at the National Chung Hsing University in Taichung in Taiwan that the AGUAAA (G=guanosine) hexamer motif could be an important element in bovine coronavirus polyadenylation and that its function is position-dependent [52].

In a 2019 publication, Jana Tvarogova and co-workers at the Institute of Medical Virology within the Justus Liebig University of Giessen in Germany report that the human coronavirus HCoV-229e nonstructural protein 8 (nsp8) has metal ion-dependent RNA 3′ terminus adenylyltransferase activity [53]. Tvarogova and co-workers speculate that that the nsp8-mediated adenylyltransferase activity is involved in the 3′ polyadenylation of viral positive-strand RNAs. Using partially double-stranded RNAs, in the presence of divalent metal ions Mg^{2+} or Mn^{2+}, very efficient adenylyltransferase activity was observed if the template strand contained a short 5′ oligo uridine sequence opposite the 3′ polyadenylation site. Notably, such uridine sequences exist in all isolated SARS-CoV-2 genomes [54].

The poly(A) tail mediates survival of coronavirus RNA

Despite the limited understanding of the SARS-CoV-2 polyadenylation process, critically, the author of this communication argues that survival of a coronavirus, that includes SARS-CoV-2, is dependent absolutely upon a patent and functioning poly(A) tail. The corollary of this argument is that functional immobilisation by therapeutic intervention of the SARS-CoV-2 poly(A) tail will kill all variants of SARS-CoV-2 at all stages in its life cycle.

The poly(A) tail is conditional for coronavirus RNA replication

Jeannie Spagnolo and Brenda Hogue in the Department of Molecular Virology and Microbiology at the Baylor College of Medicine in Houston in USA investigated the importance of the poly(A) tail in coronavirus replication [55]. Using the bovine coronavirus defective genome BCV Drep (DNA-launched self-replicating) and the murine coronavirus, mouse hepatitis virus (MHV) strain MHV-A59 defective interfering (DI) genome MHV MIDI-C, together with several mutants, they demonstrate that the poly(A) tail is an important *cis*-acting signal for coronavirus RNA replication. Notably, these studies showed that a bovine coronavirus defective RNA replicon without a poly(A) tail was unable to replicate. They acknowledge that their results accord with the results of a previous study by Lin and co-workers that showed that MHV defective genomes in which the poly(A) tail was deleted were incapable of serving as templates for negative-strand synthesis [56].

Spagnolo and Hogue state that the results of their study demonstrate that host proteins, that include poly(A) binding protein (PABP) specifically interact with the 3′-untranslated region of bovine coronavirus genomic RNA. They propose that RNAs with abbreviated poly(A) tails demonstrated diminished *in vitro* PABP binding, and that

Preprints (www.preprints.org) | NOT PEER-REVIEWED | Posted: 9 December 2022 doi:10.20944/preprints202212.0175.v1

attenuated interactions with PABP may affect RNA replication. Notably, retarded kinetics of replication were observed in all mutants.

They conclude that their results support the view whereby positive-strand RNA virus replication…. "has evolved to depend on elements of the host cell translation machinery" (Spagnolo and Hogue, 2000) [55] and that critically, their results provide additional evidence that the coronavirus poly(A) tail represents an important *cis*-acting signal for coronavirus replication.

Minor changes in poly(A) tail length exert significant effects upon gene expression and replication of coronavirus

Silvestri and coworkers in the Department of Biochemistry and Molecular Biology at the University of Florida in Gainsville, USA investigated the effect of changes in the length of the poly(A) tail upon poliovirus negative-strand RNA synthesis [59]. In their hands, they observed that increasing the poly(A) tail length by a single nucleotide resulted in an increase of negative-strand synthesis by approximately an order of magnitude, suggesting that minor changes in viral poly(A) tail length exert a significant effect on viral replication. Similar results have also been obtained with the Sindbis virus whereby for example, decreasing the poly(A) tail length by five nucleotides resulted in a greater than 70% decrease in negative-strand RNA synthesis [60].

Similarly, for coronavirus, small alterations in poly(A) tail were observed to markedly affect the efficiency of viral replication [55] and translation [58].

Consistent with the above reports of the effects of minor changes in poly(A) tail length upon virus propagation, Kim and Chang [57] propose that nsp8-mediated adenylyltransferase activity of human coronavirus HCoV-229e may extend the poly(A) tail of coronaviruses, including SARS-CoV-2 as a counter measure against the erosive attack by host deadenylases. Moreover, they additionally speculate that regulation of the length of the viral poly(A) tail is important for the maintenance of genome integrity and facilitation of translation mediated by interaction with poly(A) binding proteins, that in turn interact with translation factors to allow translation. They conclude that the viral poly(A) tail facilitates and/or mediates multiple roles in translation, decay, and replication.

The SARS-CoV-2 poly(A) tail changes length during infection

Following infection by bovine coronavirus, the length of the coronaviral poly(A) tail has been shown to vary by up to an order of magnitude throughout the infection period [52].

In a 2013 study, Hung-Yi Wu and coworkers in the Graduate Institute of Veterinary Pathobiology at National Chung-Hsing University in Taiwan observed that coronaviral poly(A) length varies throughout a the study period of one hundred and forty-four hours from viral entry [58]. Although they report that the mechanisms regulating the change in poly(A) tail length remain unknown, they propose a positive link between regulation of poly(A) tail length and coronaviral translation and replication, whereby a longer poly(A) tail is a critical determinant of successful replication.

In a later study by the same group investigated the mechanisms for synthesis of the poly(A) tail and subsequent variation in length during the infection period [52]. These new observations enable novel insights into this process whereby small changes in poly(A) tail length can affect viral replication and translation during infection [52]. Interestingly, their data additionally suggest that in the early stages of infection, poly(A) tail length below a critical number (they propose five to nine nucleotides) may attenuate the subsequent efficiency of lengthening, that in turn may compromise gene expression during infection. The corollary of these observations gives rise to an interesting speculation by the author whereby coronavirus with short "embryonic" poly(A) tails may be exquisitely vulnerable to the effects of dexrazoxane (discussed later).

Preprints (www.preprints.org) | NOT PEER-REVIEWED | Posted: 9 December 2022 doi:10.20944/preprints202212.0175.v1

Do RNA modifications regulate poly(A) tail length?

Intriguingly, Kim and Chang [57] report that they identified at least forty-one potential RNA modification sites (changes to the chemical composition of molecules post-synthesis that have the potential to alter function or stability) on SARS-CoV-2 viral transcripts. Among these modification sites, the most frequently observed motif is AAGAA. Notably, modified RNAs were shown to carry shorter poly-A tails than unmodified RNAs, suggesting an association between the internal modification and the poly(A) tail. Kim and Chang surmise that by an unknown mechanism the relationship between modification and the length of the poly(A) tail confers stability to the RNA. Moreover, they extend their reasoning to include the possibility that RNA modifications may confer additional benefit upon viral survival. That is, modifications enable evasion by virus RNA in infected tissues given that it has been reported by Karikó and coworkers that nucleoside modifications suppress the potential of RNA to activate dendritic cells. Consequently, the host cell's innate immune system may fail to adequately recognise the threat posed by viral RNA that incorporates nucleoside modification [74]. While the modifications observed in their study remain to be characterised (for example, N6-methyadenosine, 5-methylcytosine, 2′-O-methylation, deamination) they conclude that viral RNA modifications may represent an additional layer of coronavirus stability and survival that in some way is dependent upon a functional poly(A) tail.

The coronavirus poly(A) tail is a coincidence detector that regulates

translation

Tsung-Lin Tsai and co-workers at the Graduate Institute of Veterinary Pathobiology at the National Chung Hsing University in Taiwan investigated whether the coronavirus poly(A) tail functions as a so-called "coincidence detector" whereby temporally close signal inputs are interrogated providing an output that controls the functional mode of the genome as an effector of either translation or replication [61]. During coronavirus infection, the positive-strand genome must coordinate both translation and replication whereby ribosomes travel along the viral RNA in the 5′-to-3′ sense and the viral RNA polymerase travels in the opposite 3′-to-5′ sense.

Tsai and co-workers studied the interactions between the poly(A) tail, bovine coronavirus nucleocapsid protein, and poly(A) binding protein using human rectum tumour (HRT-18) cells, and human embryonic kidney (HEK-293) cells infected with bovine coronavirus.

From their observations, they construct a model whereby following infection, the poly(A) tail of the coronavirus genomic RNA interacts with poly(A) binding protein, and the translation factors eukaryotic initiation factor 4G (eIF4G) and eIF4E. This assembly results in translation. As the infection progresses there is an increase in nucleocapsid protein, which upon binding to the poly(A) tail results in a destabilisation of the above assembly and a termination of translation. With an increase in the levels of nucleocapsid protein the coronaviral RNA switches from translation to replication.

Most importantly, the results of Tsai and coworkers suggest that coronavirus nucleocapsid protein also inhibits host mRNA translation [61]. The net result is an accumulation of viral proteins with a concomitant substantial reduction by the host of protein synthesis, a phenomenon often termed "host shutoff".

In summary, the model proposed by Tsung-Lin Tsai and co-workers shows a coordinating role of the coronavirus poly(A) tail as a "coincidence detector" in harmonizing coronavirus replication and translation, together with the concomitant inhibition of host mRNA translation.

Does SARS-CoV-2 poly(A) tail form an intrinsic helical structure?

Seminal studies by Terence Tang together with Lori Passmore at the MRC Laboratory of Molecular Biology in Cambridge in the UK, suggest that eukaryote poly(A) forms an

 doi:10.20944/preprints202212.0175.v1

intrinsic base-stacked, single-stranded helical conformation that is recognized by the highly conserved Pan2 exonuclease [62]. Their work suggests that regulation of the poly(A) tail length by exonuclease-mediated deadenylation is critically dependent upon this helical conformation. The corollary of their finding is that disruption of this structure blocks the interaction of poly(A) with Pan2. If this work can be extrapolated to the poly(A) tail of SARS-CoV-2 then any intervention that disrupts this conformation-dependent interaction may have a deleterious impact upon the SARS-CoV-2 life cycle.

Destabilization of the poly(A) tail of the SARS-CoV-2 virus as a novel approach for the management of Covid-19

Reprogramming poly(A)

Hanadi Sleiman and co-workers in the Department of Chemistry and Centre for Self-assembled Chemical Structures at McGill University in Quebec, Canada studied the interaction between cyanuric acid (Figure 7) and poly(adenine), in both its DNA and RNA forms [63]. These workers showed that cyanuric acid can "reprogramme poly(A) interactions and induce the assembly of a higher-order supramolecular structure" (Avakyan et al, 2016 p. 368) [63] via both canonical and non-canonical base pairs. Because cyanuric acid contains three 2,4-dione assemblies of thymine (Figure 7) (dexrazoxane contains two 2,4-dione assemblies), these workers propose that their observations are consistent with the self-assembly of cyanuric acid with poly(adenine) strands to yield a coiling triplex formation as determined by circular dichroism and UV-visible spectroscopy.

The association between cyanuric acid and poly(adenine) studied by Sleiman and coworkers is illustrated in figures 8A, 8B, and 9. Cross-sectional plan views (Figures 8A and 8B) depict the basic units of two different self-assemblies. For comparative purposes, canonical Watson–Crick base pairing is shown in Figure A, and the proposed hexameric self-assembly that combines both canonical and non-canonical Hoogsteen base pairing as a coiling triplex formation is shown in Figure 8B. A three-dimensional plan view of the coiling triplex formation is illustrated in figure 9 (for clarity, only a single strand of poly(adenine) shown). Figure 9 depicts stacking of the adenine-cyanuric base pairs with the adenine bases (black), showing only one "full" strand with individual adenine bases mapping the positions of the other two poly(adenine) strands in the triplex.

In more recent times, Ramanarayanan Krishnamurthy and coworkers in the Department of Chemistry at the Scripps Research Institution in California, USA [70] have proposed a helicene-based supramolecular structure as an alternative to the hexameric assembly (Figure 8B) proposed by Sleiman and coworkers [63]. However, for the purposes of the present discussion it is not necessary to give undue attention to the exact nature of this interaction. Rather, what is critically important, is the observation that a nucleobase-mimicking small molecule can induce the assembly of a higher order structure with a nucleic acid in water.

Preprints (www.preprints.org) | NOT PEER-REVIEWED | Posted: 9 December 2022 doi:10.20944/preprints202212.0175.v1

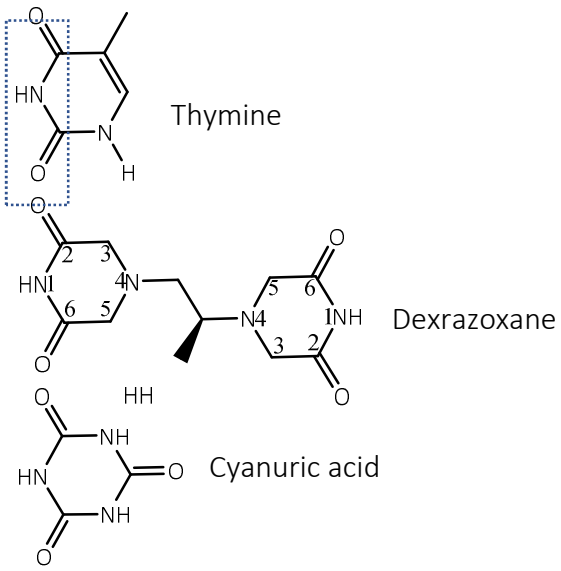

Figure 7. Each dioxopiperazine moiety of dexrazoxane contains the 2,4-dione assembly of thymine (dotted box in thymine structure), and cyanuric acid has three 2,4-dione assemblies. Reproduced under the terms of a Creative Commons Attribution License from McCormack Keith (2018) *The cardioprotective effect of dexrazoxane (Cardioxane) is consistent with sequestration of poly(ADP-ribose) by self-assembly and not depletion of topoisomerase 2B ecancer 12* 889.

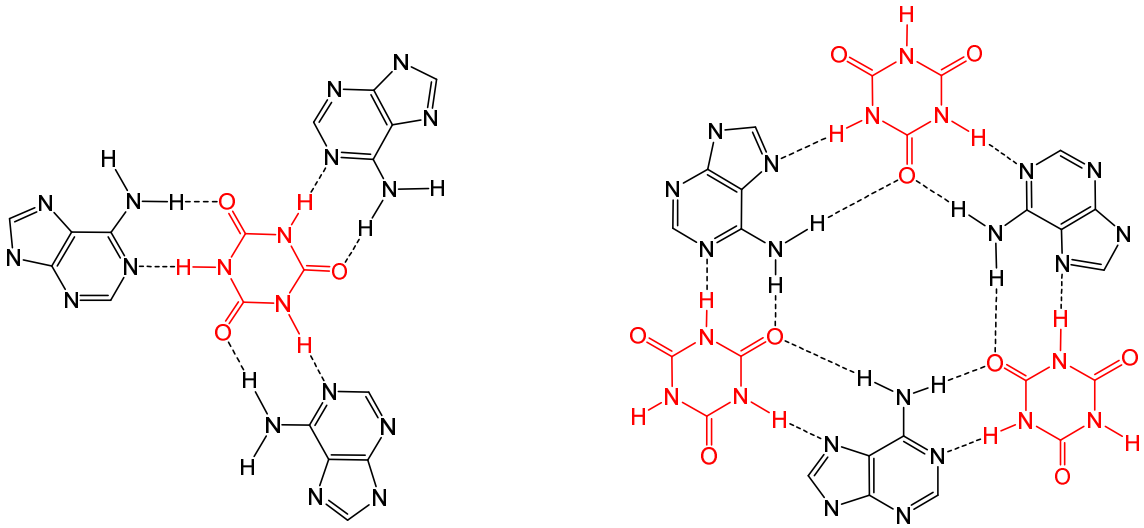

A **B**

Figure 8. Cyanuric acid monomers self-assemble with poly(adenine) strands. Canonical Watson–Crick base pairing is shown in **A** and the proposed hexameric assembly formed by both canonical and non-canonical base pairing is shown in **B**. Reproduced under the terms of a Creative Commons Attribution License from McCormack Keith (2018) *The cardioprotective effect of dexrazoxane (Cardioxane) is consistent with sequestration of poly(ADP-ribose) by self-assembly and not depletion of topoisomerase 2B ecancer 12* 889.

Preprints (www.preprints.org) | NOT PEER-REVIEWED | Posted: 9 December 2022 doi:10.20944/preprints202212.0175.v1

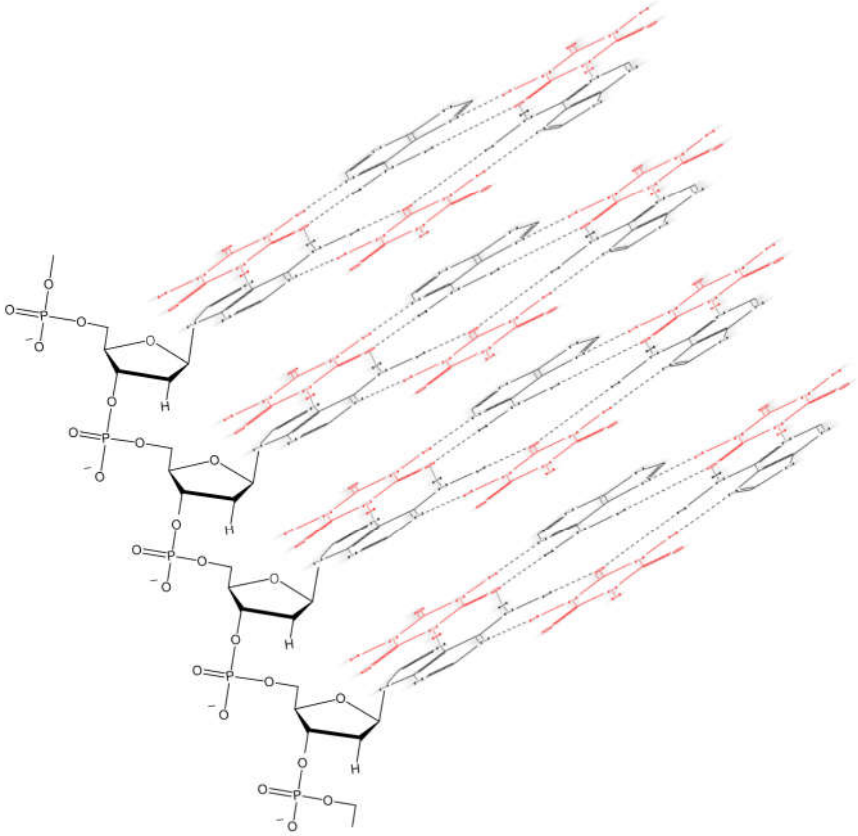

Figure 9. A three-dimensional plan view of the cyanuric acid (red)-catalysed self-assembly of a poly(adenine) triplex depicts stacking of the adenine-cyanuric base pairs with the adenine bases (black). For clarity, only a single strand of poly(adenine) is shown with individual adenine bases mapping the position of the other two strands. Reproduced under the terms of a Creative Commons Attribution License from McCormack Keith (2018) *The cardioprotective effect of dexrazoxane (Cardioxane) is consistent with sequestration of poly(ADP-ribose) by self-assembly and not depletion of topoisomerase 2B ecancer 12* 889.

Dexrazoxane and the SARS-CoV-2 poly(A) tail

Solvent entropy is a dominant driving force in stabilising the interaction beteeen dexrazoxane and poly(A)

As discussed above, in an earlier report [33], the author presented *in silico* and *in vitro* evidence in support of an association between dexrazoxane and Poly(ADP-ribose) (PAR). Given that poly(A) is closely related to PAR (Figure 5) then an interaction between dexrazoxane and poly(A) is entirely consistent with expectation. However, the model of a hybrid dexrazoxane and poly(A) supramolecular structure demonstrates an important difference to that reported for the interaction between dexrazoxane and PAR. Notably, with the dexrazoxane and poly(A) interaction, in addition to the effects of the canonical Watson-Crick base pairing (Fig 10 Upper) it is the vertical adenine-dexrazoxane-adenine stacking forces that confer robust stabilisation to the assembly (Fig 10 Middle) with solvent entropy being the dominant driving force.

Preprints (www.preprints.org) | NOT PEER-REVIEWED | Posted: 9 December 2022 doi:10.20944/preprints202212.0175.v1

Vertical stacks within the dexrazoxane-poly(A) supramolecular self-assembly are maximally-stabilized at a distance of 3.4 Å

As discussed earlier, the simulations of Mak and co-workers [45] show that as two bases approach each other to form a vertical stack there is a maximum release of energy as described by a minimum value of Gibbs free energy at a distance between the bases of 3.4 Å. This of course is the distance between stacked bases within DNA, and simulations of Mak and coworkers confirm that base stacking is a spontaneous process with maximum stability between bases at a distance of 3.4 Å. Modelling of the interaction between dexrazoxane and poly(A) shows that the distance between each vertical stack (Figure 10 Middle) is approximately 3.4 Å, affording maximal stability.

Upon entering a SARS-CoV-2-infected cell stacked parallel conformers of dexrazoxane form a symmetrical anti-parallel base pair with a complementary series of adenine bases within a poly(A) tail

Assembly within plasma of planar stacks of dexrazoxane with a vertical separation of 3.4 Å between adjacent stacks enables efficient transfer across cell membranes. Upon reaching the aqueous and charged cell interior the equilibrium shifts in favour of monomeric dexrazoxane, which, the author proposes sequesters poly(A) (Figure 10) to form a hybrid supramolecular assembly. Consumption of dexrazoxane by this interaction with SARS-CoV-2 results in a steep gradient for dexrazoxane into the cell. Moreover, the author additionally proposes that this deep compartment for the accumulation of dexrazoxane non-linearly augments the extracellular equilibrium between monomeric dexrazoxane and the lipophilic stacked dexrazoxane by a mass action shift toward the stacked structure and finally terminating in the intracellular formation of the energetically favoured hybrid supramolecular assembly between dexrazoxane and poly(A).

Conformational analysis of dexrazoxane confirms alignment between dexrazoxane and poly(A) is consistent with base pairing

Conformational analysis of dexrazoxane also reveals that at methylene carbon atoms 3 and 5 (Figure 2), each piperazine structure occupies a half-chair conformation resulting in an elevated tertiary amine nitrogen atom. Importantly, the keto group at the carbon atom in position 2 of each piperazine structure is in alignment with the tautomeric nitrogen of the primary amine group of the adenine base of each adenosine monophosphate unit of poly(A) (using the orientation depicted in Figure 10 Upper).

Base expansion within the dexrazoxane-poly(A) supramolecular self-assembly augments the stabilizing forces between stacks

The earlier *ab initio* quantum mechanics calculations and molecular modelling studies by McConnell and Wetmore in the Department of Chemistry at Mount Allison University in New Brunswick, Canada [64] provide support for Mak's observation [45] that the stability of a base stack correlates with the size of the bases. They modelled the effect upon stacking interactions in DNA attributable to an increase in the size of natural bases by covalently including a benzene ring within one or both bases within a Watson Crick pair. Interestingly, they observed that stacking interactions between base dimers were increased by up to fifty percent upon expansion of one base and by up to ninety percent upon expansion of both bases. These observations accord with the meticulous thermodynamic measurements of Guckian and co-workers in the Department of Chemistry at the University of Rochester in New York, USA who showed that in a self-complementary DNA duplex, the plot of stacking energy versus stacking surface area was robustly correlated, whereas plots of stacking energy versus either log P or dipole moment suggested little, if any association [66].

Taken together, the studies of Mak and co-workers[45], Danilov and co-workers [40] and McConnell and Wetmore [64] enable a novel insight into the self-assembly of dexrazoxane with poly(A). For the purpose of illustration, using the method of Girolami [65], the molar volume of a double-stranded adenine-uracil base pair (it is the

 doi:10.20944/preprints202212.0175.v1

demethylated form of thymine, uracil, that base pairs with adenine in RNA) (Figure 10 Lower) is approximately 192 cm^3 mol^{-1}. By contrast, using the same method, the molar volume of the adenine-dexrazoxane-adenine unit within the dexrazoxane-poly(A) supramolecular canonical structure (Figure 10 Upper and Middle) is approximately 404 cm^3 mol^{-1}, which is more than twice that of the adenine-uracil base pair within double-stranded RNA. Consequently, given that the stability of a base stack correlates with the size of the bases, then we may confidently predict the existence of significant stabilizing forces between vertically-orientated adenine-dexrazoxane-adenine stacks within the dexrazoxane-poly(A) supramolecular self-assembly (Figure 10 Upper and Middle).

A note on Hoogsteen base pairing

Additionally, dexrazoxane may catalyse the self-assembly of supramolecular structures with poly(A) through a combination of both canonical base pairing, and non-canonical Hoogsteen base pairing leading to the formation of assemblies of increased complexity (Figure 11), beyond that shown in figure 10. However, further discussion on Hoogsteen base pairs is beyond the scope of this document.

Preprints (www.preprints.org) | NOT PEER-REVIEWED | Posted: 9 December 2022 doi:10.20944/preprints202212.0175.v1

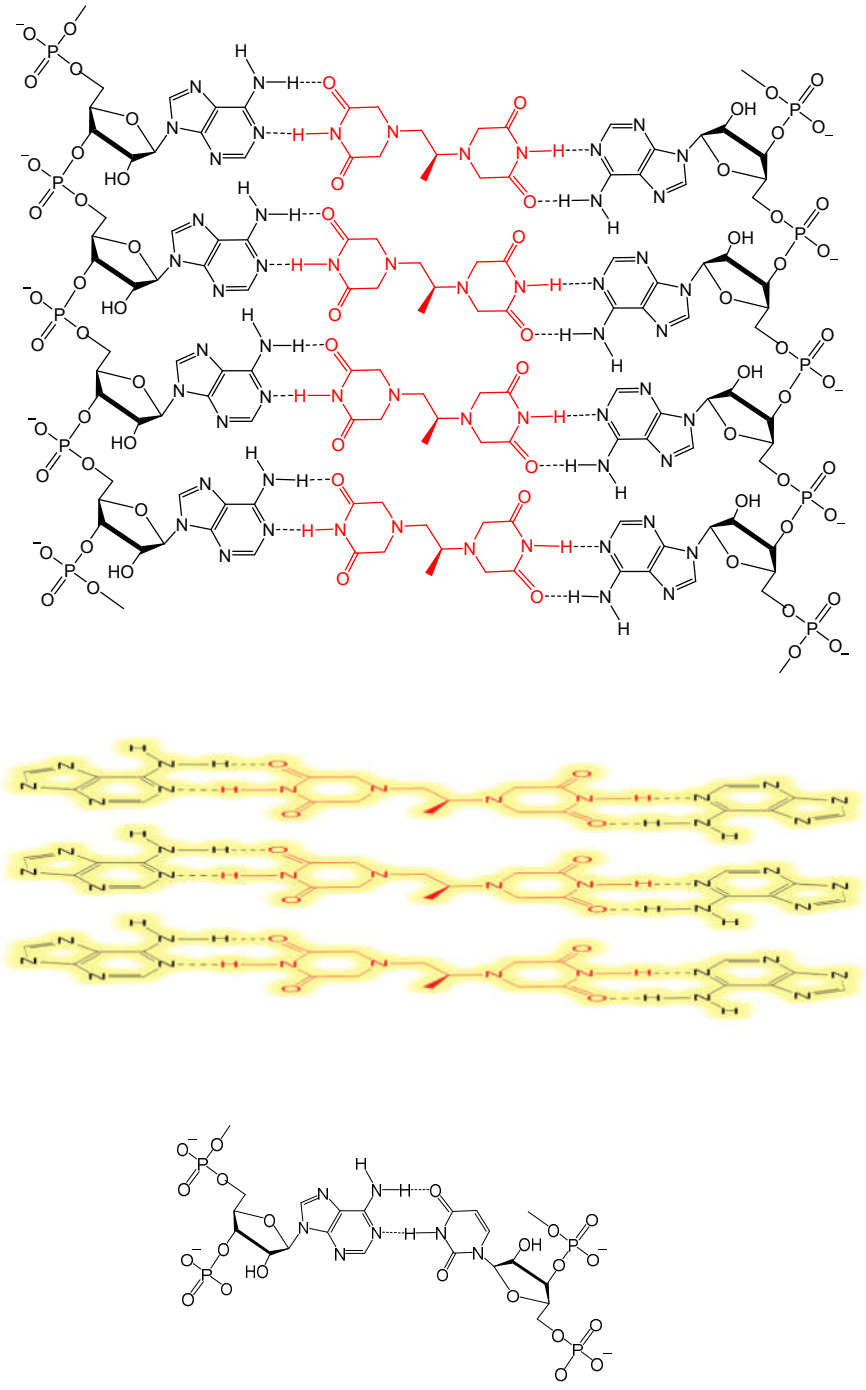

Figure 10. Dexrazoxane (red) catalyses the hybrid self-assembly of SARS-CoV-2 poly(A) tails (**UPPER**). Three adenine-dexrazoxane-adenine stacks with vertical inter-stack distance of approximately 3.4Å (**MIDDLE**). For comparison, canonical adenine-uracil base pairing is shown. It is the demethylated form of thymine, uracil, that base pairs with adenine in RNA (**LOWER**).

Preprints (www.preprints.org) | NOT PEER-REVIEWED | Posted: 9 December 2022 doi:10.20944/preprints202212.0175.v1

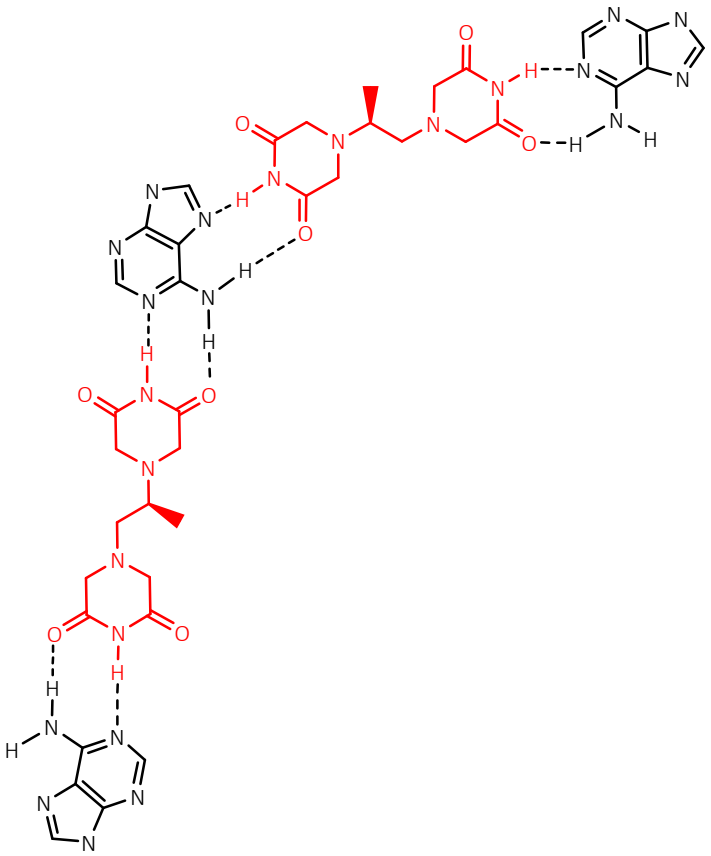

Figure 11. Dexrazoxane may additionally self-assembly with poly(A) through a combination of both canonical base pairing, and non-canonical Hoogsteen base pairing; the adenine moieties of poly(A) are shown in black. Reproduced under the terms of a Creative Commons Attribution License from McCormack Keith (2018) ***The cardioprotective effect of dexrazoxane (Cardioxane) is consistent with sequestration of poly(ADP-ribose) by self-assembly and not depletion of topoisomerase 2B*** *ecancer* ***12*** 889.

An assessment of the stoichiometry between dexrazoxane and the SARS-CoV-2 virus

Targeting the pneumocyte

The mean peak plasma concentration of dexrazoxane is reported as 36.5 μg ml^{-1} at fifteen minutes following an intravenous administration of a 500 mg m^{-2} dose. Within the age range of nineteen to forty years, using morphometric analysis, Crapo and co-workers [67] report that a human alveolar type I epithelial cell has a mean volume of 1,764.0 μm^3, and that an alveolar type II cell has a mean volume that is half that of the type I pneumocyte.

Estimating the absolute number of molecules of dexrazoxane within a pneumocyte

Applying Avogadro's number with a molecular weight for dexrazoxane of 268.27, and assuming a steady state exists, within the absolute intracellular volume of a type II pneumocyte (a primary target of SARS-CoV-2), there are approximately 10^8 dexrazoxane molecules. This figure is an overestimate to within one order of magnitude since the available cytosol volume in the pneumocyte is less than the intracellular volume by approximately 30%.

Preprints (www.preprints.org) | NOT PEER-REVIEWED | Posted: 9 December 2022 doi:10.20944/preprints202212.0175.v1

Estimating the number of individual SARS-CoV-2 RNA molecules within infected cells

Jeffrey Lee and co-workers in the Department of Biochemistry at the University of Oxford in the United Kingdom used single-molecule fluorescence *in situ* hybridisation to explore the spatial and temporal quantification of positive sense SARS-CoV-2 RNA genomes, while simultaneously visualising negative sense genomes, subgenomic RNAs, and viral proteins [68].

Using Vero E6 cells (derived from the kidney of the African green monkey and highly susceptible to SARS-Cov-2), A549-hACE2 cells (derived from human lung cancer cells that express angiotensin-converting enzyme 2 (ACE2)), and Calo-3 cells (a non-small-cell lung cancer cell that has constitutively active ErbB2/Her2) they demonstrated that single molecule fluorescence in situ hybridization is an efficient and sensitive assay with the power to detect single molecules of RNA from cells innoculated with the SARS-CoV-2 variant B.1.1.7. Importantly, the sensitivity of the assay enabled unprecedented insights into the dynamics of viral replication in infected Vero E6 cells during the first ten hours of infection.

The infected cell population showed varying gRNA levels that were classified by Lee and co-workers into three groups. The first group of 'partially resistant' cells with $<10^2$ positive sense SARS-CoV-2 RNA genome copies that showed no increase in copies burden between two and eight hours post infection (sixty percent of the population). The second group of 'permissive' cells with approximately 10^2–10^5 copies per cell showing a modest increase over time (thirty percent of the population), and the third group of 'super-permissive' cells with $>10^5$ copies per cell showing a sharp increase in gRNA copies (ten percent of the population).

Interestingly, at six hours post infection Lee and co-workers observed a high abundance of SARS-CoV-2 subgenomic RNA (that provide templates for the production of various structural and accessory proteins) compared to levels of genomic SARS-CoV-2 RNA. This rapid expansion of subgenomic RNA peaked at eight hours post infection (approximately 10^7 counts per cell) followed by a shift towards the production of genomic RNA. They interpret the high generation of subgenomic RNA as being consistent with fulfilling a critical need for an adequate supply of structural proteins in anticipation of the later appearance of genomic RNA, and the subsequent generation of new viral particles (Lee et al, 2022) [68].

Accepting that the findings by Lee and co-workers can be extrapolated to the clinical situation, then at all time points the intracellular content of dexrazoxane either matches or outnumbers the counts of both genomic and subgenomic SARS-Cov-2 counts. However, the number of individual dexrazoxane molecules needed to effectively inactivate two adjacent SARS-CoV-2 poly(A) tails remains unknown.

7. Analogues of dexrazoxane

Is dexrazoxane the most appropriate bisdioxopiperazine to target SARS-CoV-2?

ICRF-154 (Figure 12) is the demethylated analogue of dexrazoxane [69]. Although widely available for research purposes, ICRF-154 is not approved for any clinical indication. However, the absence of the methyl group results in a conformational landscape that is heavily populated with low energy linear conformers. Arguably, relative to dexrazoxane, the absence of the methyl group increases the capacity of ICRF-154 to form parallel stacks. The corollary of this assumption is that on a molar basis ICRF-154 is more potent than dexrazoxane in destabilizing the SARS-CoV-2 poly(A) tail. However, in the absence of more data, this assertion remains purely speculative.

Preprints (www.preprints.org) | NOT PEER-REVIEWED | Posted: 9 December 2022 doi:10.20944/preprints202212.0175.v1

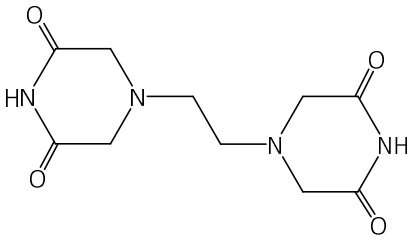

Figure 12. ICRF-154 4-[2-(3,5-dioxopiperazin-1-yl)ethyl]piperazine-2,6-dione.

8. Concluding remarks

SARS-Cov-2-infected cells represent a deep compartment for the accumulation of dexrazoxane

As proposed by the author herein, spontaneous catalysis by intracellular dexrazoxane of the formation of a hybrid self-assembly with SARS-Cov-2 poly(A) tails within infected cells, renders the virus incapable of normal function and replication. Consumption of dexrazoxane by this interaction with SARS-CoV-2 results in a steep gradient for dexrazoxane into the cell. Moreover, the author additionally proposes that this deep compartment for the accumulation of dexrazoxane non-linearly augments the extracellular equilibrium between monomeric dexrazoxane and the lipophilic stacked dexrazoxane by a mass action shift toward the stacked structure and finally terminating in the formation of the energetically favoured hybrid supramolecular assembly between dexrazoxane and poly(A). Destabilisation of the SARS-Cov-2 poly(A) tail kills the virus.

The relationship between dose of dexrazoxane or ICRF-154 and response remains to be explored.

Can dexrazoxane target other viruses?

Destabilisation of the poly(A) tail by dexrazoxane merits further attention as an intervention that may have more general application for the immobilization of viruses other than the SARS-CoV-2 virus.

9. Materials and methods

Some of the methods described below were also used in McCormack, 2018 [33] and accordingly some of the wording in the Methods section from that article have been reproduced in part [33].

Development of the association rule learning algorithm incorporating the use of antecedent surrogate variables algorithm (coded as CEME) was pioneered by McCormack Pharma in the early 1980s [75]. CEME displays exquisite sensitivity in probing natural language text for the discovery of new and interesting associations that otherwise would remain lost [33, 75].

The conformational relationship of the non-covalent interaction between dexrazoxane and poly(A), and energy minimization was explored using a modified version of Allinger's Molecular Mechanics MM2 force field. Conformational analysis with a dihedral driver was performed and minimum energy conformations were computed for dexrazoxane and ICRF-154 using Chem3D 16.0 with a minimum root mean squared gradient set to 0.1. Semi-empirical molecular orbital calculations were also undertaken using the Chem3D 16.0 tool MOPAC to eliminate unstable high energy conformers and for geometry optimisation. Conformational analysis and energy minimisation was additionally supported by the Chem3D 16.0 tool, CONFLEX (CONFLEX Corporation). Intermolecular distances were estimated using the distance measuring tool within Chem3D. Dissociation constants as pKa that were not evident within the literature were calculated using methods provided within Chemaxon (MarvinSketch).

Acknowledgements and conflicts of interest:

The author declares that there are no conflicts or competing interests.

The earlier association rule mining, *in silico* modelling, and *in vitro* investigations reported in McCormack, 2018 [33] were supported by a grant from Clinigen Healthcare Ltd., Burton-On-Trent, UK. The author is the first inventor on a lapsed patent application: McCormack K and George PL (2015) PAR Inhibition. Patent Application Number PCT/GB2015/054026; Publication number WO2016051213 A1.

The author acknowledges the meticulous efforts by Dr Kenneth J Ritchie at Liverpool John Moores University in the investigation of the effects of dexrazoxane upon poly(ADP-ribose)-induced release of apoptosis-inducing factor from isolated mitochondria that were reported in McCormack, 2018 [33].

Special thanks are expressed to Peter L George FIBMS MBA MSc, entrepreneur, industrialist and friend, for introducing the author to dexrazoxane, for his suggestions in improving previously reported work [33], and for critically reading an early draft of the present manuscript.

Funding: No funding.

References

1. Hasinoff BB, Kuschak TI, Yalowich JC, and Creighton AM. A QSAR study comparing the cytotoxicity and DNA topoisomerase II inhibitory effects of bisdioxopiperazine analogs of ICRF-187 (dexrazoxane) *Biochem Pharmacol* 1995; 50(7) Sept 28 953-958. https://doi.org/10.1016/0006-2952(95)00218-O PMID: 7575679

2. McCormack K. Data on file 2022; May; McCormack Pharma, Stirling house, London, UK

3. Herman EH, Mhatre RM, and Chadwick DP. Modification of some of the toxic effects of daunorubicin (NSC-82,151) by pretreatment with the antineoplastic agent ICRF 159 (NSC-129,943) *Toxicol App lPharmacol* 1974; 27(3) Mar; 517- 526. https://doi.org/10.1016/0041-008X(74)9 0031-3

4. Herman EH, Ardalan B, Bier C, Waravdekar V, and Krop S. Reduction of daunorubicin lethality and myocardial cellular alterations by pre-treatment with ICRF-187 in Syrian golden hamsters *Cancer Treat Rep* 1979; 63(1) Jan; 89–92. PMID: 421236

5. Herman EH, and Ferrans VJ. Influence of vitamin E and ICRF-187 on chronic doxorubicin cardiotoxicity in miniature swine *Lab Invest* 1983; 49(1) Jul; 69–77. PMID: 6408310

6. Herman EH, Ferrans VJ, Young RS, and Hamlin RL. Pretreatment with ICRF-187 allows a marked increase in the total cumulative dose of doxorubicin tolerated by beagle dogs *Drugs Exp Clin Res* 1988; 14(9); 563–570. PMID: 3147886

7. Herman EH, and Ferrans VJ. Preclinical animal models of cardiac protection from anthracycline-induced cardiotoxicity *Semin Oncol* 1998; 25(4 Suppl 10) Aug; 15–21. PMID: 9768819

8. Prescribing information Summary of Product Characteristics. CARDIOXANE 500 mg powder for solution for infusion 2018; Jan; Marketing Authorisation holder Clinigen Healthcare Ltd, Burton-on Trent, Staffordshire, DE14 2WW, UK

9. Dexrazoxane. PubChem 2022; May; National Library of medicine, National Center for Biotechnology Information, Bethesda, MD, 20894, USA

10. Zinecard. Dexrazoxane for Injection. Reference ID:3152327; 2012; Jun; Pharmacia & Upjohn Co, Division of Pfizer Inc, NY, NY 10017, USA

11. Dexrazoxane for Injection. 2005; Jun; Ben Venue Laboratories, Inc, Bedford, OH 44146, USA

12. Totect. Dexrazoxane for Injection. 2020; Dec; RxList, Rxlist.com

13. Savene. Dexrazoxane. Scientific Discussion. Committee for Medicinal Products for Human Use, European Medicines Agency 2006

14. Dexrazoxane. DrugBank. 2022; May; Drugbank.com

15. Yardley, PA 19067, USA Totect. Dexrazoxane for Injection. Reference ID: 4700835; 2020; Nov; Clinigen, Inc,

16. Cardioxane. Dexrazoxane. ChemSpider. 2022; Chemspider.com

17. Jordan K, Behlendorf T, Mueller F, and Schmoll H-J. Anthracycline extravasation injuries: management with dexrazoxane *Ther Clin Risk Manag* 2009; 5(2) Apr; 361-366. https://doi.org/10.2147/TCRM.S3694 PMID: 19536310

18. Srivastava R. Theoretical Studies on the Molecular Properties, Toxicity, and Biological Efficacy of 21 New Chemical Entities *ACS Omega* 2021; 6(38) Sept 28; 24891-24901.https://doi.org/10.1021/acsomega.1c03736 PMID: 34604670

19. Ethanol. DrugCentral. 2021; Oct; drugcentral.org

20. Ethanol. Suprabank. Pubchem. 2022; suprabank.org

21. Ethanol. Chakraborty N, Das S, Saha D, and Mondal S. Material surface – analyte interactions with similar energy rates vary as univariate quadratic function of topological polar surface area of analytes; CSIR Central Glass and Ceramic Research Institute, 196, Raja S. C. Mullick Road, Kolkata-700032, India

22. Ethanol. PubChem 2022; May; National Library of medicine, National Center for Biotechnology Information, Bethesda, MD, 20894, USA

23. Urea. PubChem 2022; May; National Library of medicine, National Center for Biotechnology Information, Bethesda, MD, 20894, USA

24. Glycerol. PubChem 2022; May; National Library of medicine, National Center for Biotechnology Information, Bethesda, MD, 2089

25. Finkelstein A. Water and nonelectrolyte permeability of lipid bilayer membranes *J Gen Physiol* 1976; 68(2) Aug 1; 127-135. https://doi.org/10.1085/jpg.68.2.127 PMID: 956767

26. Orbach E, and Finkelstein A. The nonelectrolyte permeability of planar lipid bilayer membranes *J Gen Physiol* 1980; 75(4) Apr 1; 427-436. https://doi.org/10.1085/jgp.75.4.427 PMID: 7381427

27. Gray ALH, Steren CA, Haynes IW, Bermejo GA, Favretto F, Zweckstetter M, and Do TD. Structural Flexibility of Cyclosporine A is Mediated by Amide *Cis-Trans* Isomerization and the Chaneleonic Roles of Calcium *J Phys Chem B* 2021; 125(5) Feb 1; 1378-1391. https://doi.org/10.1021/acs.jpcb.0c11152 PMID:33523658

28. Batista MLS, Neves CMSS, Carvalho PJ, Gani R, and Coutinho JAP. Chameleonic Behaviour of Ionuc Liquids and Its Impact on the Estimation of Solubility Parameters *J Phys Chem B* 2011; 115(44) Sept 28; 12879-12888. https://doi.org/10.1021/jp207369g PMID: 21954861

29. Cavasin AT, Hillisch A, Uellendah F, Schneckener S, and Göller AH. Reliable and Performant Identification of Low-Energy Conformers in the Gas Phase and Water *J Chem Inf Model* 2018; 58(5) May 29; 1005-1020. https://doi.org/10.1021/acs.jcim.8b00151 PMID: 29717870

30. Davies RH, Sheard B, and PJ Taylor. Conformation, partition, and drug design *J Pharm Sci* 1979; 68(3) Mar; 396-397. https://doi.org/10.1002/jps.2600680345 PMID:423143

31. Gaillard P, Carrupt P-A, and Testa B. The conformation-dependent lipophilicity of morphine glucuronides as calculated from their molecular lipophilicity potential *Bioorg Med Chem Lett* 1994; 4(5) Mar 10; 737-742. https://doi.org/10.1016/S0960-894X(01)80191-8

32. Carrupt PA, Testa B, Bechalany A, el Taylor N, Descas P, and Perrissoud D. Morphine 6-glucuronide as molecular chameleons with unexpected lipophilicity *J Med Chem* 1991; 34(4) Apr 1; 1272-1275. https://doi.org/10.1021/jm00108a005 PMID: 2016703

33. McCormack K. The cardioprotective effect of dexrazoxane (Cardioxane) is consistent with sequestration of poly(ADP-ribose) by self-assembly and not depletion of topoisomerase 2B *Ecancermedicalscience* 2018; 12 Dec 20; 889. https://doi.org/10.3332/ecancer.2018.889 PMID: 30792806

34. Zhu Q, Lu Y, He X, Liu T, Chen H, Wang F, Zheng D, Dong H, and Ma J. Entropy and Polarity Control the Partition and Transportation of Drug-Like Molecule in biological Membrane *Sci Rep* 2017; 7(1) Dec 18; 17749. https://doi.org/10.1038/S41598-017-18012-7 PMID: 29255188

35. Isayez O, Furmanchuk A, Shishkin OV, Gorb L, and Leszcynski J. Are isolated nucleic acid bases really planar? A Car-Parrinello molecular dynamics study *J Phys Chem B* 2007; 111(13) Apr 5; 3476-3480. https://doi.org/10.1021/jp070857j PMID: 17388492

36. Xiao S, and Liang H. The conformational flexibility of nucleic acid baes paired in gas phase: a Car-Parrinello molecular dynamics study *J Chem Phys* 2012; 136(20) May 28; 205102. https://doi.org/10.1063/1.4720352 PMID: 22667590

37. Wang S, and Schaefer 3rd HF. The small planarization barriers for the amino group in the nucleic acid bases *J Chem Phys* 2006; 124(4) Jan 28; 044303. https://doi.org/10.1063/1.2162538 PMID: 16460158

38. Sychrovsky V, Foldynova-Trantirkova S, Spackova N, Robeyns K, Van Meervelt L, Blankenfeldt W, Vokacova Z, Sponer J, and Trantirek L. Revisiting the planarity of nucleic acid bases: Pyramidilization at glycosidic nitrogen in purine bases is modulated by orientation of glycosidic torsion *Nucleic Acids Research* 2009; 37(21) Sept 28; 7321-7331. https://doi.org/10.1093/nar/gkp783 PMID: 19786496

39. Yakovchuk P, Protozanova E, and Frank-Kamenetskii MD. Base-stacking and base-pairing contributions into thermal stability of the DNA double helix *Nucleic Acids Res* 2006; 34(2) Jan 31; 564-574. https://doi.org/10.1093/nar/gkj454 PMID: 16449200

40. Danilov VI, Dailidons V, van Mourik T, and Fruchtl HA. A study of nucleic acid base-stacking by the Monte Carlo method: Extended cluster approach *Cent Eur J Chem* 2011; 9(4) Aug; 720-727. https://doi.org/10.2478/s11532-011-0056-0

41. Luo R, Gilson HS, Potter MJ, and Gilson MK. The physical basis of nucleic acid base stacking in water *Biophys J* 2001; 80(1) Jan; 140-148. https://doi.org/10.1016/S0006-3495(01)76001-8 PMID: 11159389

42. Langlet J, C Giessner-Prettre, Pullman P, Claverie p, and Piazzola D. Purine-water interactions in base stacking *Int J Quantum Chem* 1980; 18(2) Aug; 421-437. https://doi.org/10.1002/qua.560180212

43. Martel P. Base Crystallization and base Stacking in Water *FEBS J* 1979; 96(2) May; 213-422. https://doi.org/10.1111/j.1432-1033.1979.tb13031.x

44. Moghaddam MJ, Kanbara K, Hozumi S, Inaki Y, and Takemoto K. Syntheses and Photochemical reactions of Bis-Thymine Derivatives *Polymer J* 1990; 22(5) May 1; 369-380. https://doi.org/10.1295/polymj.22.369

45. Mak CH. Unraveling Base Stacking Driving Forces in DNA *J Phys Chem B* 2016; 120(26) Jul 7; 6010-6020. https://doi.org/10.1021/acs.jpcb.6b01934 PMID: 27045853

46. Cafferty BJ, Gállego I, Chen MC, Farley KI, Eritja R, and Hud NV. Efficient self-assembly in water of long noncovalent polymers by nucleobase analogues *J Am Chem Soc* 2013; 135(7) Feb 20; 2447-2450. https://doi.org/10.1021/ja312155v PMID: 23394182

47. Zhou Z, and Bong D. Small-molecule/polymer recognition triggers aqueous-phase assembly and encapsulation *Langmuir* 2013; 29(1) Jan 8; 144-150. https://doi.org/10.1021/la304457y PMID: 23205819

48. Grimme S. Do special noncovalent pi-pi stacking interactions really exist? *Angew Chem Int Ed Engl* 2008; 47(18) Apr 14; 3430-3434. https://doi.org/10.1002/anie.200705157 PMID: 18350534

49. Vekilov PG, Feeling-Taylor AR, Yau ST, and Petsev D. Solvent entropy contribution to the free energy of protein crystallization *Acta Crystallogr D Biol Crystallogr* 2002; 58(Pt 10 Pt1) Sept 26; 1611-1616. https://doi.org/10.1107/s0907444902014312 PMID: 12351872

50. Lipshultz SE, Scully RE, Lipsitz SR, Sallan SE, Silverman LB, Miller TL, et al. Assessment of dexrazoxane as a cardioprotectant in doxorubicin-treated children with high-risk acute lymphoblastic leukaemia: long-term follow-up of a prospective, randomised, multicentre trial *Lancet Oncol* 2010; 11(10) Oct 1; 950-961. https://doi.org/10.1016/S1470-2045(10)70204-7 PMID: 20850381

51. Lipshultz SE, Anderson LM, Miller TL, Gerschenson M, Stevenson KE, and Neuberg DS. Impaired mitochondrial function is abrogated by dexrazoxane in doxorubicin-treated childhood acute lymphoblastic leukemia survivors *Cancer* 2016; 122(6) Mar 15; 946-953. https://doi.org/10.1002/cncr.29872 PMID: 26762648

52. Peng Y-H, Lin C-H, Lin CN, Lo C-Y, Tsai T-L, and Wu H-Y. Characterization of the Role of Hexamer AGUAAA and Poly(A) Tail in Coronavirus Polyadenylation *PLoS One* 2016; 11(10) Oct 19; e0165077. https://doi.org/10.1371/journal.pone.0165077

53. Tvarogova J, Madhugiri R, Bylapudi G, Ferguson LJ, Karl N, and Ziebuhr J. Identification and Characterization of a human Coronavirus 229E Nonstructural Protein 8-associated RNA 3′-Terminal Adenylyltransferase Activity *J Virol* 2019; 93(12) Jun15; e00291-19. https://doi.org/10.1128/JVI.00291-19 PMID: 30918070

54. Brant AC, Tian W, Majerciak V, Yang W, and Zheng Z-M. SARS-CoV-2: from its discovery to genome structure, transcription, and replication *Cell Biosci* 2021; 11(1) Jun 19; 136. https://doi.org/10.1186/s13578-021-00643-z PMID: 34281608

55. Spagnolo JF, and HogueBG. Host Protein Interactions with the 3′ End of Bovine Coronavirus RNA and the Requirement of the Poly(A) Tail for Coronavirus defective Genome Replication *J Virol* 2000; 74(11) Jun 1; 5053-5065. https://doi.org/10.1128/jvi.74.11.5053-5065.2000 PMID: 10799579

56. Lin YJ, Liao CL, and Lai MM. Identification of the cis-acting signal for minus-strand synthesis of a murine coronavirus: implications for the role of minus-strand RNA in RNA replication and transcription *J Virol* 1994; 68(12) Dec 1; 8131-8140. https://doi.org/10.1128/JVI.68.8131-8140.1994. PMID: 7966604

57. Kim D, Lee J-Y, Jeong-Sun Yang, Kim JW, Kim VN, and Chang H. The Architecture of SARS-CoV-3 Transcriptome *Cell* 2020; 181(4) May 14; 914-921.e10. https://doi.org/10.1016/j.cell.2020.04.011 PMID: 32330414

58. Wu H-Y, Ke T-Y, Liao W-Y, and Chang N-Y. Regulation of Coronaviral Poly(A) Tail Length during Infection *PLoS One* 2013; 8(7) July 29; e70548. https://doi.org/10.1371/journal.pone.0070548 PMID: 23923003

59. Silvestri LS, Parilla JM, Morasco BJ, Ogram SA, and Flanegan JB. Relationship between poliovirus negative-strand RNA synthesis and the length of the 3′ poly(A) tail *Virology* 2006; 345(2) Feb 20; 509-519. https://doi.org/10.1016/j.virol.2005.10.1019

60. Hardy RW, and Rice CM. Requirements at the 3′ end of the sindbis virus genome for efficient synthesis of minus-strand RNA *J Virol* 2005; 79(8) Apr 15; 4630-4639. https://doi.org/10.1128/JVI.79.8.4630-4639.2005 PMID: 15795249

61. Tsai T-L, Lin C-H, Lin C-N, Lo C-Y, and Wu H-Y. Interplay between the Poly(A) Tail, Poly(A)-Binding Protein, and Coronavirus Nucleocapsid Protein Regulates Gene Expression of Coronavirus and the Host Cell *J Virol* 2018; 92(23) Dec 1; e01162-18. https://doi.org/10.1128/JVI.01162-18 PMID:30209168

62. Tang TTL, and Passmore LA. Recognition of Poly(A) RNA through Its Intrinsic Helical Structure *Cold Spring Harb Symp Quant Biol* 2020; 84 Jan 1; 21-30. https://doi.org./10.1101/sqb.2019.84.039818 PMID: 32295929

63. Nicole Avakyan, Greschner AA, Aldaye F, Serpell CJ, Toader V, Petitjean A, and Sleiman HF. Reprogramming the assembly of unmodified DNA with a small molecule *Nat Chem* 2016; 8(4) Apr; 368-376. https://doi.org./10.1038/nchem.2451 PMID: 27001733

64. McConnell TL, and Wetmore SD. How do size-expanded DNA nucleobases enhance duplex stability? Computational analysis of the hydrogen-bonding and stacking ability of xDNA bases *J Phys Chem B* 2007; 111(11) Mar 22; 2999-3009. https://doi.org.10.1021/jp0670079 PMID:17388411

65. Girolami GS. A Simple "Back of the Envelope" Method for Estimating the Densities and Molecular Volumes of Liquids and Solids *J Chem Edu* 1994; 71(11) Nov 1;962-964. https://doi.org/10.1021/ed071p962

66. Guckian KM, Schweitzer BA, Ren RX-F, Sheils CJ, Tahmassebi DC, and Kool ET. Factors Contributing to Aromatic Stacking in Water: Evaluation in the Context of DNA *J Am Chem Soc* 2000; 122(10) Feb 10; 2213-2222. https://doi.org/10.1021/ja9934854 PMID: 20865137

67. Crapo Jd, Barry BE, Gehr P, Bachofen M, and Weibel ER. Cell number and cell characteristics of the normal human lung *Am Rev Resp Dis* 1982; 126(2) Aug; 332-337. https://doi.org/10.1164/arrd.1982.126.2.332 PMID: 7103258

68. Lee JY, Wing PAC, Gala DS, Noerenberg M, Jarvelin AJ, Titlow J, Zhuang X, palmalux N, Louisa Iselin et al. Absolute quantitation of individual SARS-CoV-2 RNA molecules provides a new paradigm for infection dynamics and variant differences *eLife* 2022; e74153 https.//doi.org/10.7554/eLife.74153

69. ICRF-154. PubChem 2022; May; National Library of medicine, National Center for Biotechnology Information, Bethesda, MD, 20894, USA

70. Alenaizan A, Fauche K, Krishnamurthy R, and Sherrill CD. Noncovalent Helicene Structure between Nucleic Acids and Cyanuric Acid *Chemistry* 2021; 27(12) Feb 24; 4043-4052. https://doi.org/10.1002/chem.202004390 PMID: 33174300

71. Yang NJ, and Hinner MJ. Getting Across the Cell Membrane: An Overview for Small Molecules, Peptides, and Proteins *Methods Mol Biol* 2015; 1266 Jun 2; 29-53. https://doi.org/10.1007/978-1-4939-2272-7_3 PMID: 25560066

72. Matsson P, and Kihlberg J. How Big Is Too Big for Cell Permeability? *J Med Chem* 2017; 60(5) Feb 24; 1662-1664. https://doi.org/10.1021/acs.jmedchem.7b00237 PMID: 28234469

73. David L, Wenlock M, Barton P, and Ritzen A. Prediction of Chameleonic Efficiency *ChemMedChem* 2021; 16(17) Sep 6; 2669-2685. https://doi.org/10.1002/cdmc.202100306 PMID: 34240561

74. Kariko K, Buckstein M, Houping N, and Weissman D. Suppression of RNA Recognition by Toll-like Receptors: The Impact of Nucleoside Modification and the Evolutionary Origin of RNA *Immunity* 2005; 23(2) Aug; 165-175. https://doi.org/10.1016/j.immun.2005.06.008 PMID: 1611635

75. https://mccormackpharma.com